

STUDY ON PROPAGATION LAW OF ACOUSTIC EMISSION SIGNALS ON ANISOTROPIC WOOD SURFACE

TINGTING DENG, SHUANG JU, MINGHUA WANG, MING LI
SOUTHWEST FORESTRY UNIVERSITY
CHINA

(RECEIVED OCTOBER 2020)

ABSTRACT

In order to explore the influence of wood's anisotropic characteristics on Acoustic Emission (AE) signals' propagation, the law of AE signals' propagation velocity along different directions was studied. First, The center of the specimen's surface was took as the AE source, then 24 directions were chose one by one every 15° around the center, and 2 AE sensors were arranged in each direction to collect the original AE signals. Second, the wavelet analysis was used to denoise the original AE signals, then the AE signals were reconstructed by Empirical Mode Decomposition (EMD). Finally, time difference location method was utilized to calculate AE signals' propagation velocity. The results demonstrate that AE signals' propagation velocity has obvious feature of quadratic function. In the range of 90°, as the angle of propagation direction increases, the propagation velocity of the AE signals presents a downward trend.

KEYWORDS: Wood, acoustic emission, propagation velocity, empirical mode decomposition.

INTRODUCTION

Acoustic Emission Technology (AET) is an initiative non-destructive testing method, which has been widely used in damage detection of concrete structures and rocks. Noorsuhada (2016) and Noorsuhada et al. (2014) applied AET to evaluate the fatigue damage of reinforced concrete structures. Muhamad et al. (2006) calculated the propagation velocity of AE signals on the surface of concrete beams utilizing the time difference method. The experiments results demonstrate that as the distance between the source and sensor increases, the wave velocity decreases. Based on this, Noorsuhada et al. (2013) studied the AE signals' propagation velocity inside reinforced concrete beams making use of waveform analysis. In addition, Yin and Tang (2005) applied AET to study the change law of the AE fractal features and fractal values with time in the rock failure process, and established the fractal model of AE intensity. Antonaci et al. (2011) took masonry as specimens and used AET to evaluate the damage evolution and mechanical properties of masonry.

In recent years, AET has been gradually utilized in nondestructive testing of wood and composites (Niemz et al. 2009, Krauss and Kudela 2011). Diakhate et al. (2017) explored the internal crack propagation of wood with the help of AET. Yoon et al. (2015) adopted AET to investigate the AE signals' features of layered fracture of carbon fiber reinforced polymer. Wu et al. (2014) and Zhuoping (2009) took flawless and defective timber as the specimens, and summarized the specimens' microstructure evolution under bending failure through recording the AE signals' characteristics. What's more, several types of damage were identified according to different feature parameters. Li et al. (2018) found that wavelet analysis can accurately locate the AE signals' source. Nasir et al. (2019) applied AE sensors to collect stress wave data and created a neural network model to classify thermal modified materials.

AET has been extensively put into use in wood nondestructive testing, but the research on the anisotropic propagation features of AE signals was rare. Heo et al. (2004) detected the propagation velocity of AE signals in anisotropic rocks under triaxial compression. Zhang et al. (2018) extracted the fractal characteristics of anisotropic shale in Brazil with AE principle. Nozawa et al. (2014) utilized wavelet analysis to classify the features of AE signals during the crack propagation of anisotropic composite materials SiC. The tests results demonstrate that wavelet analysis is effective for AE signal classification. Ciampa and Meo (2010a,b) adopted continuous wavelet transform to analysis the time domain and frequency domain of the AE signals from the surface of carbon fiber composites. The conclusion proves that this method can reduce the location error result full and realize AE source location. Ju et al. (2018, 2019) explored the propagation law of AE signals from the surface of *Pinus massoniana* plywood by wavelet analysis. An artificial AE source was produced by snapping 2H pencil lead in the experiment. Although there are few studies with respect to the effects of wood anisotropy on AE signal propagation law, the above researches are enlightening .

This paper took rubber wood (*Hevea brasiliensis* Muell. Arg) as the specimen to study the frequency features and propagation law of the AE signals spreading along different directions, while the AE signals came from the same AE source. First, the direction of bonding gap on the specimen surface was set as the standard. The AE signals was produced by snapping the pencil lead at the location of the AE source, and the raw AE signals were collected counterclockwise and clockwise respectively. Then, AE signals were extracted from the original signals containing noises through wavelet analysis. After that the AE signals were decomposed into several Intrinsic Mode Function (IMF) components by EMD algorithm. The correlation between each IMF components and its original AE signal was analyzed, at the same time, the correlation coefficient was calculated. In addition, the frequency analysis was carried out on the component with the largest correlation coefficient. Thus the characteristic frequency of the signals can be confirmed. Finally, the propagation velocity was calculated according to the time difference location method. The function between the propagation velocity of AE signals on specimen's surface and the angles of propagation directions was constructed through polynomial fitting method.

MATERIALS AND METHODS

Materials

The specimen is laminated finger-joint board made by rubber wood. The size of the specimen is $2000 \times 1000 \times 10$ mm (length \times width \times thickness) and the moisture content is 8-12%. In order to ensure the quality of AE signals, a 4-channel AE signal acquisition system was built by the data acquisition card (NI USB-6366) and LabVIEW software. What's more, single-ended resonant AE sensors (SR150) with an acquisition frequency range of 20-220 kHz were connected to preamplifiers (PAI, gain set at 40 dB). According to Shannon Sampling Theorem, the sampling frequency of each channel was set to 500 kHz, and the acquisition voltage range of each channel was from -5V to +5V.

Methods

Firstly, a circular area with a radius of 350 mm on the surface of the specimen was selected, and according to the American Society for Testing Materials standards (ASTM E976-99), AE signals were generated by snapping 0.3 mm-diameter 2H pencil leads at point A which was in the center of the circle. The angle between the pencil leads and the surface of the specimen were 30° and the length of each snap of pencil lead was 2.5 mm. Secondly, the direction of the bonding gap of the specimen was set to 0° and the AE signals were and clockwise collected every 15° starting from 0° as shown in Fig. 1. In addition, 10 measurements were realized at each direction. After the AE signals were processed by the designed algorithms, the AE signals' propagation velocity in each direction was obtained. Therefore, the law of AE signals' propagation velocity in different directions was studied.

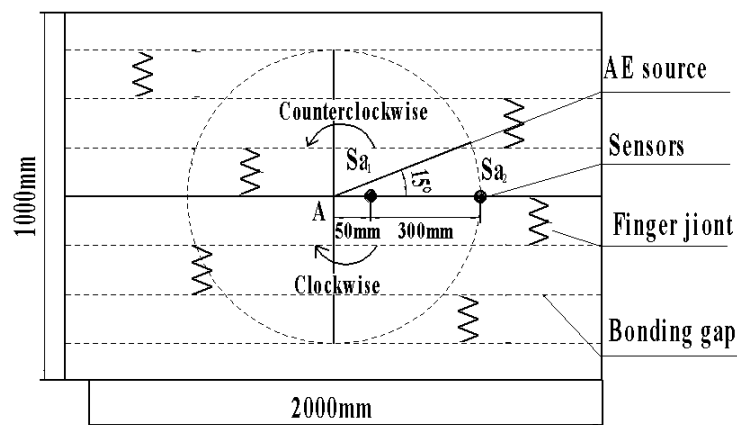


Fig. 1: Sketch of the experiment scheme.

Due to the influence of the propagation paths, measurement system and environmental noises of AE signals, the output electric signals of the AE sensors are a kind of typical nonlinear and non-stationary random signal (Jiang and Xu 2017). Therefore the wavelet analysis method was used to denoise the original AE signals. After that the AE signals were reconstructed by EMD algorithm (Huang 2000). The process of EMD decomposition was as follows:

Firstly, local maximum points and minimum points of the AE signals $x(t)$ were chosen, and the upper envelope curve $y_0(t)$ formed by the maximum points and the lower envelope curve $z_0(t)$ formed by the minimum points were fitted by cubic spline interpolation. Then the average value

$m_1(t)$ of the upper and lower envelope curves was calculated:

$$m_1(t) = \frac{y_0(t) + z_0(t)}{2} \quad (1)$$

After the instantaneous average $m_1(t)$ was subtracted from the original AE signals $x(t)$, a new sequence $v_1(t)$ was got:

$$v_1(t) = x(t) - m_1(t) \quad (2)$$

Secondly, the judgment conditions of IMF include two parts. One condition is that the number of extreme points and zero-crossing points must be equal or differ by at most 1. The other one is that the average value of the upper and lower envelope curves should be zero. If the conditions were satisfied, then $v_1(t)$ was the first IMF component of $x(t)$ named $imf_1(t)$ and that meant $imf_1(t) = v_1(t)$. The original signals minus the component equaled that $h_1(t) = x(t) - imf_1(t)$. If the conditions were not satisfied, took $v_1(t)$ as a new data to repeat the above steps. IMF components were presented in turn, $imf_2(t)$, $imf_3(t)$, ... $imf_n(t)$; $h_2(t) = h_1(t) - imf_2(t)$, ..., $h_n(t) = h_{n-1}(t) - imf_n(t)$. When $h_n(t)$ was a single sequence which no longer contained any modal information; it was the residual term of the original AE signals. After decomposition the original AE signals could be expressed as:

$$x(t) = \sum_{i=1}^n imf_i(t) + h_n(t) \quad (3)$$

Finally, the IMF component which had the largest correlation coefficient with the raw signals was adopted as the final AE signal and the principal component which was analyzed to identify the characteristic frequency of AE signal.

RESULTS AND DISCUSSION

Features of AE signals on the specimen's surface

There were too many AE signals collected in different directions to list all of them. Actually they were generated by the same AE source and their features of time and frequency domain were similar. Therefore, the signals collected by the sensor Sa₁, which were parallel to the bonding gap and closest to point A were taken as an example. Fig. 2a was a graph of the original signals' time domain. It can be seen from the graph of the original signals' frequency domain as shown in Fig. 2b that the frequency of main component signals Sa₁ was 2 kHz, which was very low. For AE source was generated instantaneously through snapping pencil lead, its energy was weak and the original signals contained a lot of noise signals. So the raw signals needed to be denoised by wavelet analysis.

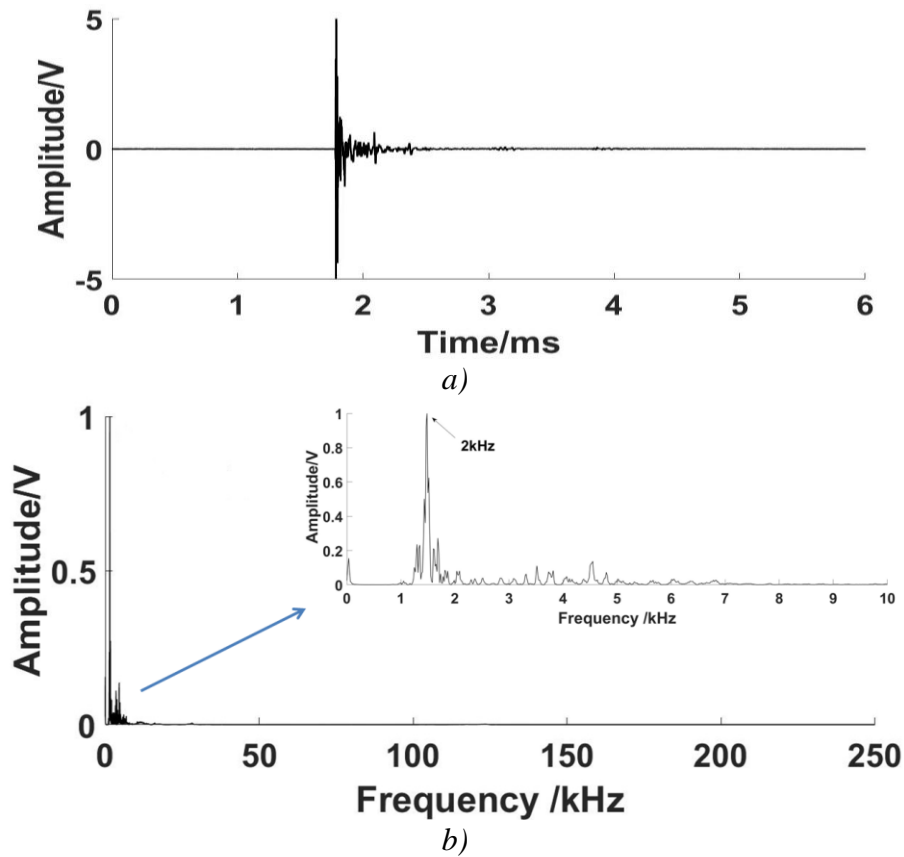


Fig. 2: The original AE signals: a) the signal of time domain. b) the signal of frequency domain.

After noises reduction, the AE signals were decomposed by EMD. Then 15 IMF components and 1 residual term were obtained as shown in Fig. 3. In order to identify the principal component, each component was made correlated analysis with the original signals. The IMF6 component's correlation coefficient was 0.1146 and the components after it had smaller correlation coefficient. So only the first 6 components were listed in Tab. 1. As shown in Tab. 1, the IMF3 component had the largest correlation coefficient; therefore it was the principal component. Then, the IMF3 component was analyzed in the frequency domain and its spectrum is showed in Fig. 4. In order to highlight the signals' proportion, the signals were normalized during analysis. Fig. 4 indicates that the AE signals' energy concentrates on the frequency of 35 kHz.

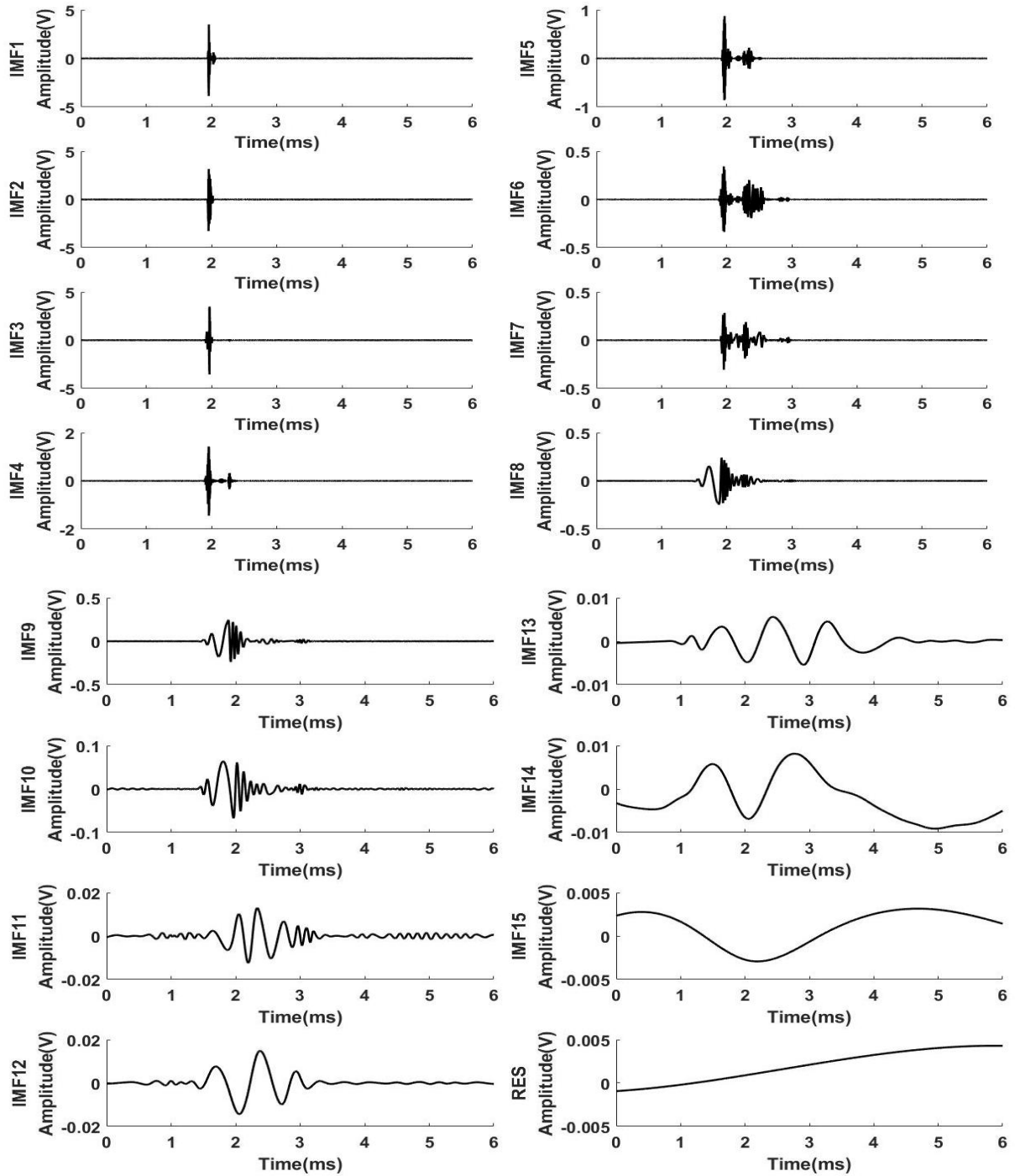


Fig. 3: The IMF components and residual term decomposed by EMD.

Tab. 1: The correlation coefficients of IMF with the original signals.

Intrinsic Mode Function	IMF1	IMF2	IMF3	IMF4	IMF5	IMF6
Correlation Coefficient	0.4952	0.5748	0.8951	0.3573	0.2657	0.1146

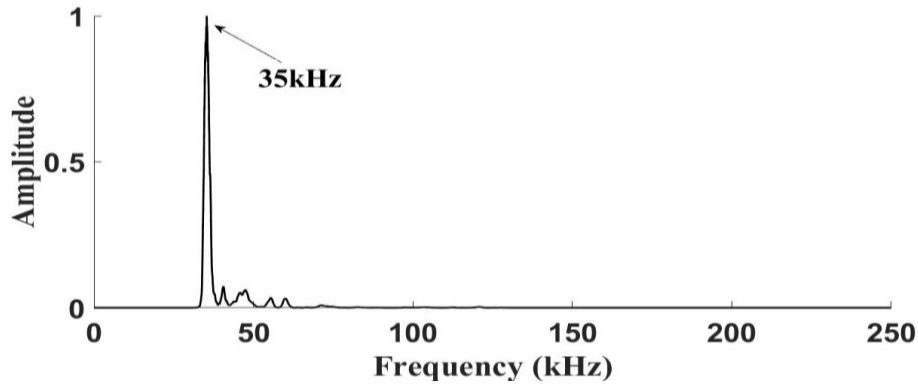


Fig. 4: The AE signals' reconstruction spectrum.

Propagation law of AE signals in different directions

The time difference location method and cross-correlation analysis method were used to calculate the propagation velocity of AE signals. Firstly, the sensors were arranged at points which were 50 mm away from point A. The relative distances between the 2 AE sensors were all set as $\Delta s = 300$ mm as shown in Fig. 1. Then the AE signals cost different time to reach the 2 AE sensors and the time differences named Δt were calculated by cross-correlation analysis method. The cross-correlation function mainly describes the degree of similarity between 2 signals (Asari et al. 2014, Mao et al. 2002). The cross-correlation function of the signals $j(t)$ and $k(t)$ were defined as:

$$R_{jk}(\tau) = \lim \frac{1}{T} \int_0^T j(t)k(t + \tau) dt \quad (4)$$

According to the definition of cross-correlation function, if when $\tau = \tau_0$, the absolute value $|R_{jk}(\tau_0)|$ of the cross-correlation function equals the maximum value. The signal $k(t)$ is most similar to signal $j(t)$ after it is translated τ_0 units along the time axis. Therefore, the time difference Δt can be figured out indirectly by cross-correlation function. The propagation velocity of AE signals was calculated as: $v = \Delta s / \Delta t$. In order to minimize the impact of the random affection of the test, 10 independent tests were made in each direction. The calculation results were showed in Tab. 2 and Tab. 3. As can be seen, when the angle between AE signals' propagation direction and the direction of bonding gap was 90° , the minimum propagation velocity was about $810 \text{ m}\cdot\text{s}^{-1}$, and when the angle was 180° , the maximum propagation velocity was about $1410 \text{ m}\cdot\text{s}^{-1}$. The angle was taken as a variable and the AE signals' average velocity function of Tab. 2 and Tab. 3 was fitted by a quadratic polynomial method. The results were as follows:

$$v_1(\alpha_1) = 0.063\alpha_1^2 - 11.22\alpha_1 + 1388.1 \quad (5)$$

$$v_2(\alpha_2) = 0.068\alpha_2^2 - 11.90\alpha_2 + 1400.7 \quad (6)$$

where: v_1 and v_2 are the AE signals' average velocity ($\text{m}\cdot\text{s}^{-1}$); α_1 and α_2 are angles ($0^\circ - 180^\circ$).

Tab. 2: The average velocity from 0° to 180° counterclockwise.

Angles (°)	Velocity (m·s ⁻¹)										Average velocity (m·s ⁻¹)	Standard deviation
0	1451.4	1462.5	1451.4	1478.9	1462.5	1351.4	1430.6	1562.5	1351.4	1451.4	1445.4	57.8
15	1120.4	1181.1	1102.9	1111.1	1250.0	1271.9	1227.4	1230.0	1171.9	1207.4	1187.4	57.1
30	1056.3	980.4	1041.7	1049.0	986.8	1141.7	1056.3	1041.7	1056.3	1041.7	1035.2	41.6
45	986.8	986.8	986.8	1094.9	986.8	986.8	986.8	986.8	1102.9	1094.9	1020.0	50.8
60	937.5	1041.7	1034.5	1027.4	1041.7	937.5	1027.4	937.5	937.5	937.5	986.0	48.7
75	881.3	850.0	850.0	993.4	902.9	902.9	885.0	986.8	993.4	986.8	923.3	57.2
90	750.0	806.0	753.8	810.8	897.2	810.8	852.3	721.2	897.2	852.3	815.2	57.6
105	990.2	892.9	897.2	955.2	801.3	902.9	895.2	932.9	897.2	885.2	905.0	47.0
120	910.8	939.3	990.5	1010.0	953.8	915.2	1039.3	1090.5	915.2	910.8	967.5	59.6
135	1171.9	1041.7	1043.4	1139.9	1037.5	1171.9	1041.7	1043.4	1139.9	1037.5	1086.9	57.3
150	1136.4	1045.0	1153.8	1153.8	1145.0	1041.7	1145.0	1153.8	1103.8	1145.0	1122.3	41.9
165	1071.9	1192.8	1239.3	1227.4	1194.9	1182.8	1171.9	1162.8	1227.4	1192.8	1186.4	44.9
180	1415.8	1415.1	1462.5	1404.3	1304.3	1401.9	1393.1	1428.6	1339.7	1415.1	1398.0	42.7

Tab 3: The average velocity from 0° to 180° clockwise.

Angles (°)	Velocity (m·s ⁻¹)										Average velocity (m·s ⁻¹)	Standard deviation
0	1455.4	1462.5	1351.4	1478.9	1562.5	1451.4	1530.6	1562.5	1562.5	1451.4	1486.9	64.5
15	1050.0	1086.8	1060.5	1093.4	1150.0	1150.0	1160.5	1086.8	1260.5	1193.4	1149.2	62.5
30	1171.9	1102.9	1011.1	1031.7	1000.0	1020.0	1102.9	1011.1	1031.7	931.7	1041.5	63.9
45	954.0	924.0	1049.0	1162.8	1049.0	954.0	924.0	1029.0	1019.0	1032.8	1021.8	69.6
60	943.4	937.5	1102.9	1111.1	937.5	931.7	1020.4	943.4	937.5	931.7	979.7	68.3
75	924.0	986.8	881.3	950.0	1049.0	962.8	949.0	962.8	881.3	850.0	939.7	55.3
90	742.6	781.3	781.3	867.1	777.2	785.3	819.7	862.1	867.1	777.2	806.1	42.6
105	923.6	887.5	936.4	1039.7	973.8	893.8	887.8	883.8	895.2	921.3	924.3	46.9
120	1111.1	980.4	937.5	937.5	986.8	924.0	980.4	1111.1	980.4	986.8	993.6	62.7
135	943.4	994.9	992.9	903.6	1020.4	1094.9	1020.4	1094.9	943.4	1094.9	1010.4	65.2
150°	1102.9	1102.9	1250.0	1250.0	1239.7	1102.9	1111.1	1111.1	1102.9	1239.7	1161.3	68.3
165°	1381.1	1330.6	1330.6	1371.9	1190.5	1234.5	1330.6	1330.6	1271.9	1190.5	1296.3	66.6
180°	1405.8	1415.1	1402.5	1392.5	1504.3	1501.9	1415.1	1428.6	1385.8	1405.1	1425.7	40.3

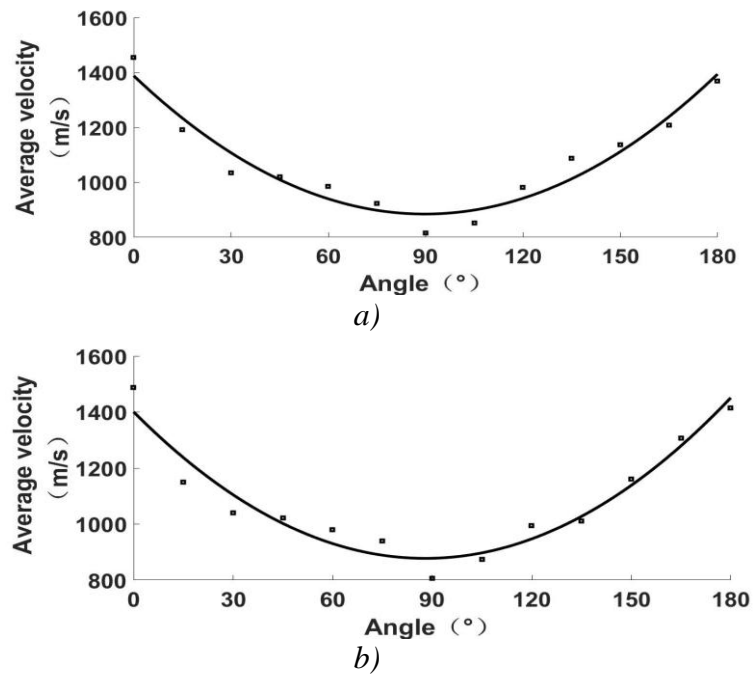


Fig. 5: The fitting curves of average velocity and angles: a) angles from 0° to 180° counterclockwise, b) angles from 0° to 180° clockwise.

As shown in Fig. 5, the propagation velocity of AE signal varies in different directions due to the influence of propagation paths and adhesive. The AE signals' propagation velocity both decreases first and then increases when the angles change clockwise and counterclockwise from 0° to 180° . But comparing Fig. 5a with Fig. 5b, it can be seen that the propagation velocity of the same AE source was almost the same in two opposite directions of the same line.

CONCLUSIONS

This paper is a preliminary exploration of the propagation law of AE signals within anisotropy wood. The AE source was produced on the anisotropy wood specimen's surface by snapping pencil lead and the AE signals' features and propagation velocity in different direction was studied through wavelet analysis and EMD. The results show that the AE signals' feature frequencies mainly concentrate around 35 kHz and the AE signals' propagation velocity both decreases first and then increases when the angle of propagation direction increases clockwise and counterclockwise from 0° to 180° . The propagation velocity along the bonding gap is the maximum and the minimum velocity appears in the orientation perpendicular to the bonding gap. Thus, it provides data for the research of the AE source's localization on the wood's surface and it has reference value for the AE source's localization of other anisotropic materials.

ACKNOWLEDGEMENTS

The authors are grateful for the support of the China Natural Science Foundation (NO: 31760182, 31100424) and Department of Education of Yunnan Provincial (NO: 2020Y0376 NO: 2021J0158).

REFERENCES

1. Antonaci, P., Bocca, P.G., Masera, D., 2011: Fatigue crack propagation monitoring by acoustic emission signal analysis. *Key Engineering Materials* 465: 370-373.
2. Asari, D., Hasegawa, H., Kanai, H., 2014: Improvement of myocardial displacement estimation using subkernels for cross correlation between ultrasonic RF echoes. *Japanese Journal of Applied Physics* 53(7S): 07-21.
3. Ciampa, F., Meo, M., 2010a: Acoustic emission source localization and velocity determination of the fundamental mode A0 using wavelet analysis and Newton-based optimization technique. *Smart Materials and Structures* 19(4): 27-45.
4. Ciampa, F., Meo, M., 2010b: A new algorithm for acoustic emission localization and flexural group velocity determination in anisotropic structures. *Composites Part A: Applied Science and Manufacturing* 41(12): 1777-1786.
5. Diakhate, M., Bastidas-Arteaga, E., Moutou, P.R., 2017: Cluster analysis of acoustic emission activity within wood material: Towards a real-time monitoring of crack tip propagation. *Engineering Fracture Mechanics* 180: 254-267.
6. Heo, J.S., Lee, C.I., Jeon S.K., 2004: Measurement of acoustic emission and source location considering anisotropy of rock under triaxial compression. *Key Engineering Materials* 270-273:1574-1579.
7. Jiang, Y., Xu, F., 2017: A novel acoustic emission source location method in the crane based on EEMD-fast ICA. *Journal of Mechanics Engineering and Automation* (7): 17-25.
8. Huang, N.E., 2000: New method for nonlinear and nonstationary time series analysis: empirical mode decomposition and Hilbert spectral analysis. *Proceedings of SPIE - The International Society for Optical Engineering* 4056: 197-209.
9. Ju, S., Li, X.C., Luo, T.F., 2018: Characteristics of acoustic emission signals on the surface of Masson Pine glulam with wavelet analysis method. *Journal of Northeast Forestry University* 46(08): 86-92.
10. Ju, S., Li, X.C., Luo, T.F., 2019: Study on the anisotropic propagation of acoustic emission signal on *Pinus massoniana* plywood surface. *Journal of Forestry Engineering* 4(02): 48-53.
11. Krauss, A., Kudela, J., 2011: Ultrasonic wave propagation and Young's modulus of elasticity along the grain of Scots pine wood (*Pinus sylvestris* L.) varying with distance from the pith. *Wood Research* 56(4): 479-488.
12. Li, Y., Yu, S.S., Dai, L., 2018: Acoustic emission signal source localization on plywood surface with cross-correlation method. *Journal of Wood Science* 64(2): 78-84.
13. Mao, J.D., Hundal, L.S., Thompson, M.L., Schmidt-Rohr, k., 2002: Correlation of poly(methylene) -rich amorphous aliphatic domains in humic substances with sorption of a nonpolar organic contaminant, phenanthrene. *Environmental Science & Technology* 36(5): 929-936.
14. Muhamad, B.N., Pullin, R., Holford, K.M., Lark, R., 2006: A practical investigation into acoustic wave propagation in concrete structures. *Advanced Materials Research* 13-14: 205-212.

15. Nasir, V., Nourian, S., Avramidis, S., 2019: Stress wave evaluation by accelerometer and acoustic emission sensor for thermally modified wood classification using three types of neural networks. *European Journal of Wood and Wood Products* 77(1): 45-55.
16. Niemz, P., Brunner, A.J., Walter, O., 2009: Investigation of the mechanism of failure behaviour of wood based materials using acoustic emission analysis and image processing. *Wood Research* 54(2): 49-62.
17. Noorsuhada, M.N., 2016: An overview on fatigue damage assessment of reinforced concrete structures with the aid of acoustic emission technique. *Construction & Building Materials* 112: 424-439.
18. Noorsuhada, M.N., Ibrahim, A., Muhamad, B.N., Hamidah, M.S., Soffian, N.M.S., Shahiron, S., 2014: Diagnostic of fatigue damage severity on reinforced concrete beam using acoustic emission technique. *Engineering Failure Analysis* 41: 1-9.
19. Noorsuhada, M.N., Muhamad, B.N., Ibrahim, A., 2013: An investigation of an acoustic wave velocity in a reinforced concrete beam from out-of plane and in plane sources. *Intech* 171-188.
20. Nozawa, T., Ozawa, K., Asakura, Y., 2014: Evaluation of damage accumulation behavior and strength anisotropy of NITE SiC/SiC composites by acoustic emission, digital image correlation and electrical resistivity monitoring. *Journal of Nuclear Materials* 455(1-3): 549-553.
21. Wu, Y., Shao, Z.P., Wang, F., 2014: Acoustic emission characteristics and felicity effect of wood fracture perpendicular to the grain. *Journal of Tropical Forest Science* 26(4): 522-531.
22. Yin, X.G., Li, S.L., Tang, H.Y., 2005: Study on strength fractal features of acoustic emission in process of rock failure. *Chinese Journal of Rock Mechanics Engineering* 24(19): 3512-3516.
23. Yoon, S.J., Chen, D., Han S.W., 2015: AE analysis of delamination crack propagation in carbon fiber-reinforced polymer materials. *Journal of Mechanical Science and Technology* 29(1): 17-21.
24. Zhang, S.W., Shou, K.J., Xian, X.F., 2018: Fractal characteristics and acoustic emission of anisotropic shale in Brazilian tests. *Tunnelling & Underground Space Technology* 71(5): 298-308.
25. Zhuoping, S., 2009: Acoustic emission characteristics of damage and fracture process of wood and felicity effect. *Scientia Silvae Sinicae* 45(2): 86-91.

TINGTING DENG, SHUANG JU, MINGHUA WANG, MING LI*
SOUTHWEST FORESTRY UNIVERSITY
SCHOOL OF MACHINERY AND TRANSPORTATION
KUNMING 650224, CHINA

*Corresponding author: swfu_lm@swfu.edu.cn